

Many-body quantum Monte Carlo study of 2D materials: cohesion and band gap in single-layer phosphorene

T. Frank,¹ R. Derian,² K. Tokár,² L. Mitas,³ J. Fabian,^{1,*} and I. Štich^{2,4,5,†}

¹*University Regensburg, Institute for Theoretical Physics, 93040 Regensburg, Germany*

²*Center for Computational Materials Science, Institute of Physics, Slovak Academy of Sciences, 84511 Bratislava, Slovakia*

³*Department of Physics, North Carolina State University, Raleigh, NC 27695-8202*

⁴*Institute of Informatics, Slovak Academy of Sciences, 845 07 Bratislava, Slovakia*

⁵*Department of Natural Sciences, University of Ss. Cyril and Methodius, 917 01 Trnava, Slovakia.*

Quantum Monte Carlo (QMC) is applied to obtain the fundamental (quasiparticle) electronic band gap, Δ_f , of a semiconducting two-dimensional (2D) phosphorene whose optical and electronic properties fill the void between graphene and 2D transition metal dichalcogenides. Similarly to other 2D materials, the electronic structure of phosphorene is strongly influenced by reduced screening, making it challenging to obtain reliable predictions by single-particle density functional methods. Advanced GW techniques, which include many-body effects as perturbative corrections, are hardly consistent with each other, predicting the band gap of phosphorene with a spread of almost 1 eV, from 1.6 to 2.4 eV. Our QMC results, from infinite periodic superlattices as well as from finite clusters, predict Δ_f to be about 2.4 eV, indicating that available GW results are systematically underestimating the gap. Using the recently uncovered universal scaling between the exciton binding energy and Δ_f , we predict the optical gap of 1.75 eV that can be directly related to measurements even on encapsulated samples due to its robustness against dielectric environment. The QMC gaps are indeed consistent with recent experiments based on optical absorption and photoluminescence excitation spectroscopy. We also predict the cohesion of phosphorene to be only slightly smaller than that of the bulk crystal. Our investigations not only benchmark GW methods and experiments, but also open the field of 2D electronic structure to computationally intensive but highly predictive QMC methods which include many-body effects such as electronic correlations and van der Waals interactions explicitly.

I. INTRODUCTION

Two-dimensional (2D) materials have already revolutionized science, and have the potential to revolutionize technology due to their unique electronic, optical, thermal, spin, and magnetic properties.^{1–7} Remarkably, 2D materials cover a wide range of electronic structures. The electronic properties range from metallic single atom layers of palladium and rhodium,⁸ semimetallic graphene,³ semiconducting transition metal dichalcogenides,⁵ to insulating wide-gap h-BN.⁶ Crucial for device applications are materials with a proper band gap. Layered black phosphorus (BP) features fundamental band gaps in the range of 0.3–2 eV, bridging semimetallic graphene and transition metal dichalcogenides.⁹ This range is specifically important for optoelectronic, photovoltaic, photocatalytic, fiber optic telecommunications, and thermal imaging applications.¹⁰

A single layer of black phosphorus—phosphorene—comprises sp^3 bonded phosphorus atoms forming an anisotropic puckered honeycomb lattice, see Figure 1. The three-fold bonding coordination implies that each phosphorus atom has a lone pair orbital which makes phosphorene reactive to air.⁹ This oxidation degradation is eliminated by capping or encapsulating phosphorene

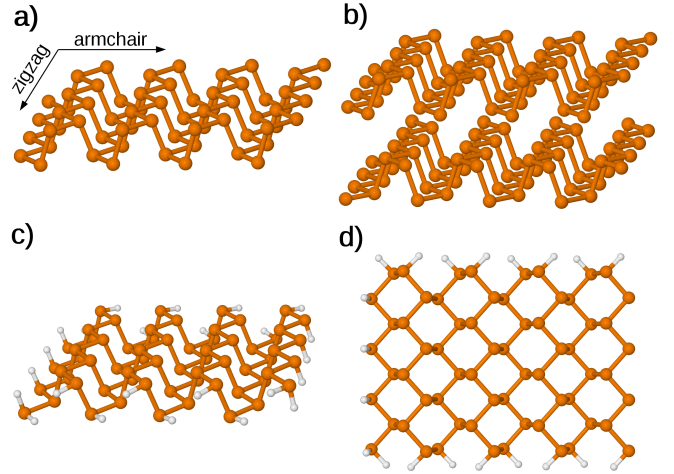


FIG. 1. Atomic structure of a) single-layer and b) few-layer phosphorene. Characteristic armchair and zigzag directions are indicated in a). Side and top views of a 4×4 cluster approximant, with saturated edge bonds, are presented in c) and d), respectively.

with(in) an insulator.

Black phosphorus features a direct band gap at the Γ point, all the way from single-layer phosphorene up to bulk. However, and this makes phosphorene particularly attractive, there are several ways to manipulate the gap. (i) First, the gap varies with the number of

* jaroslav.fabian@ur.de

† ivan.stich@savba.sk

TABLE I. Comparison of selected experimental and computed fundamental (Δ_f) and optical (Δ_o) gaps and exciton binding energies, in [eV], in unstrained single-layer phosphorene. STS, PL, PLES, and OA stand for scanning tunneling spectroscopy, photoluminescence, photoluminescence excitation spectroscopy, and optical absorption, respectively. The experimental samples correspond to exfoliation onto different substrates (Si, SiO₂, sapphire) and were studied either freshly prepared or capped by h-BN layer. G_0 and W_0 imply that the Green's function and screened Coulomb repulsion in the GW approach are calculated non-self-consistently. In GW calculations, the exciton binding energies, where quoted, were calculated in the GW-BSE (Bethe-Salpeter equation) approach.¹¹ GGA means generalized gradient approximation, H hybrid DFT functional. The present results appear in bold: DFT with GGA (PBE¹²) and H functional (B3LYP¹³) and DMC (upper two entries correspond to the periodic system with B3LYP and PBE nodal hypersurfaces, respectively, while the bottom entry to the cluster system with B3LYP treatment). The curly brace indicates compound value due to the cluster upper limit property, see the text. The star at the exciton binding energy means estimation as $\Delta_b = 0.27\Delta_f$.¹⁴

Δ_f										Δ_o											
DFT	DFT	GW_0	GW_0	GW_0	GW_0	G_0W_0	G_0W_0	G_0W_0	G_0W_0	DMC	exp.	exp.	exp.	exp.							
GGA	H	GGA	H	GGA	GGA	GGA	GGA	GGA	GGA	GGA/H	STS	PLES	PL	OA							
1.5 ¹⁵		<div><div><div>2.68±0.10</div><div>2.54±0.12</div><div>2.41±0.17</div></div><div>}</div><div>2.4</div></div>								2.0 ¹⁶	2.2±0.1 ²³	2.1±0.02 ²⁴ , 1.6 ²⁵									
0.8 ¹⁵	1.9 ¹⁶											2.4 ¹⁷	2.3 ¹⁸	2.3 ¹⁹	2.0 ^{19,20}	1.8 ¹⁴	1.6 ²¹	2.1 ²²	2.0±0.04 ²⁴ , 1.5 ² 1.7 ²⁶		
0.8	1.7											1.3±0.02 ²³									
Δ_b																					
-	-	-	-	0.9 ¹⁸	-	0.8 ²⁰	0.5 ¹⁴	-	0.8 ²²	\approx 0.65*	-	0.9±0.12 ²³	-	-							

layers and therefore band engineering techniques can be readily applied. Exfoliation of layers from the bulk BP is straightforward,^{1,2,27} see Fig. 1, due to predominantly van der Waals interlayer bonds.²⁸ While in the bulk the gap is about 0.3 eV, it increases towards about 2 eV (we argue for 2.4 eV) in single-layer phosphorene.¹⁰ (ii) Next, phosphorene can sustain large in-plane compressive/tensile strains in excess of about 10%, compared to just some 2% in the bulk.²⁹ This strain engineering is predicted to affect the band gap by $\approx \pm 50\%$.³⁰ Finally, (iii) the gap of phosphorene is predicted to be strongly susceptible to the dielectric environment.^{2,10,26}

Assuming that the fundamental (quasiparticle) band gap Δ_f depends on the dielectric that protects it against degradation, can we infer from experiments some key characteristics about pristine phosphorene providing thus the benchmark for both experiment and theory? Two established facts make the answer positive. (a) The dielectric environment affects both the fundamental gap, as well as the exciton binding energy, Δ_b .³¹ Remarkably, the difference, $\Delta_o = \Delta_f - \Delta_b$, which is the optical gap, is essentially unaffected by the dielectric.^{23,32–36} (b) Recently, a universal linear scaling between the exciton binding energy and the fundamental gap, $\Delta_b \approx 0.27\Delta_f$ was predicted based on many examples from the 2D realm¹⁴ (see also the predecessor¹⁸), including phosphorene. Combining these two observations, (a) and (b), allows to estimate Δ_o from a calculation of Δ_f on a *pristine* 2D material, namely $\Delta_o \approx 0.73\Delta_f$, and compare with experimental Δ_o obtained from an *encapsulated* or *capped* sample.

Let us now turn to the existing experimental and theoretical state-of-the-art in determining the electronic gap(s) of single-layer phosphorene. Table I shows a rather comprehensive selection of measured and calculated fun-

damental and optical gaps, as well as exciton binding energies for phosphorene. Photoluminescence is often contaminated by defect emission, as is also evidenced by the scatter of the measured values for Δ_o . Most reliable is optical absorption. A recent experiment²⁶ has reported $\Delta_o \approx 1.73$ eV, for phosphorene encapsulated in hBN. This value would lead to $\Delta_f \approx 2.4$ eV for pristine phosphorene, according to the above mentioned linear scaling. Similarly, it would suggest the exciton binding energy, Δ_b , of about 0.65 eV. Certainly both (a) and (b) observations are not exact, so the above estimates of Δ_f and Δ_b would carry a scatter of perhaps 10% or so. If we next look at the photoluminescence excitation spectroscopy data for phosphorene on silicon oxide,³⁷ the obtained fundamental gap is $\Delta_f \approx 2.2 \pm 0.1$ eV. Considering the influence of the oxide, it is reasonable to deduce from this experiment that the fundamental gap of free-standing phosphorene is 0.1–0.2 eV greater, that is, 2.3–2.4 eV.³⁷

On the theory side, we see from Tab. I that single-particle density functional methods predict, unsurprisingly, too low and strongly method-dependent values for Δ_f . Inclusion of GW corrections¹¹ is essential to bring the gaps closer to 2 eV. However, various GW approximants (G_0W_0 or GW_0) give different values coming from different implementations, ranging from 1.6 eV to 2.4 eV. The largest value, 2.4 eV, which would be consistent with the aforementioned optical absorption experiments, is obtained by using a hybrid functional.³⁷ However, the same implementation predicts 0.6 eV band gap for bulk BP³⁷ (experimental value is 0.3 eV), making it clear that there is a limited predicting power from this calculation. As for the exciton binding energies, predictions (see Tab. I) range from 0.5 to 1 eV, again with little consensus in

both theory and experiment. The experimental value of 0.9 eV³⁷ is likely affected by the optical edge of 1.3 eV of the emission peak (compare to 1.73 eV of the absorption experiment²⁶).

To obtain accurate bounds and reliable estimates of the band gap of phosphorene, we propose to employ the quantum Monte Carlo (QMC) method. QMC is an efficient, albeit computationally demanding^{38,39} way to benchmark electronic structure calculations in condensed matter.^{40–42} Indeed, this method has been applied to compute band gaps in three-dimensional systems,⁴⁰ clusters,⁴³ and nanoparticles.⁴⁴ In the 2D realm it was already used to obtain reference binding energies of 2D bilayers,^{28,45} but thus far has not been systematically employed to obtain electronic structure parameters.

Here we report QMC calculations for the fundamental band gap of single-layer phosphorene. We use both the periodic lattice as well as supercell approaches, to demonstrate convergence and consistency. The accuracy of the ground-state properties is evidenced by calculating cohesion, which differs little from the bulk value. We stress that our QMC calculation is the full method, not relying on phenomenological interactions. In fact, *we solve the Schrödinger equation for hundreds of electrons* interacting mutually as well as with the lattice ions, to obtain the ground and excited states needed for the band gap calculation. Finally, we note that the knowledge of the band gap of phosphorene is important not only on its own right as a fundamental electronic quantity of a potentially technologically relevant material, but it is crucial also for building effective theories such as tight-binding²¹ and k-p models.⁴⁶ We believe that our adaptation of QMC methods will open the way for this powerful technique to investigations of electronic structures of 2D systems, which are inherently prone to strong interactions and require careful considerations.

II. SIMULATION TECHNIQUES

The band gap Δ_f was determined from both extended and cluster approximants with lattice parameters fixed to the experimental values in the black phosphorus crystal. In fact, it was shown that the experimental lattice parameters agree with the lattice parameters determined by QMC methods within the error bars²⁸. The gap Δ_f was extracted as the singlet-singlet vertical excitation energy. Here $\Delta_f \approx E_v^{ss} = E_1^s - E_0^s$, with E_0 and E_1 being, respectively, the ground- and the first excited-states obtained by fixed-node QMC³⁸ not allowing any relaxation of the DFT nodal hypersurfaces due to the HOMO→LUMO electron excitation; no vibronic effects are included. The fixed-node approximation is the only fundamental approximation in the electronic structure QMC.³⁸

In the periodic setup the E_0 and E_1 were computed from DMC (diffusion Monte Carlo) energies in the fixed-node approximation using the VMC (variational Monte

Carlo) trial wave functions with the nodal hypersurfaces determined by two different sets of DFT orbitals: the generalized gradient approximation PBE¹² (PBE/DMC) and hybrid B3LYP¹³ (B3LYP/DMC), at the Γ -point of the Brillouin zone, optimizing the short-range correlations of the Jastrow factor.³⁸ The consistency check using both PBE and B3LYP DFT nodal hypersurfaces was deemed important as at the DFT level the HOMO-LUMO gaps of the two DFT functionals differ by ≈ 1 eV, see Table I. The Yeh-Berkowitz⁴⁷ modification in the 3D Ewald summation technique for systems with a slab geometry that are periodic in two dimensions and have a finite length in the third dimension, was adopted. We cross checked in detail that this agrees with an alternative derivation of Ewald sums for 2D slab geometries.⁴⁸ In the cluster setup we used the B3LYP¹³ (B3LYP/DMC) nodal hypersurfaces.

Finite-size scaling towards the thermodynamic limit was performed for a series of 1×1 to 6×6 series of $L \times L$ periodic approximants, see Fig. 1 a), and for 4×4 and 5×5 H-terminated cluster approximants, assuming a linear scaling with $1/N$, where $N = 4 \times L \times L$ is the number of P atoms. Our approach corresponds to quasi-exact many-body treatment, to within the fixed-node approximation, of the 2D electron polarizability entering the equations for Δ_f .¹⁴ The ground-state energy E_0 was also used to determine the cohesion energy. More details can be found in Supplementary Material (SM).

III. RESULTS AND DISCUSSION

Periodic supercells. Our finite-size diffusion Monte Carlo (DMC) scaling study of Δ_f is shown in Fig. 2 a). Although in 3D periodic calculations typical QMC extrapolations from supercells to bulk behave as $1/N$ where N is the number of atoms in the supercell, in the 2D slab systems the issue is more complicated.⁴⁸ The strong periodic Coulomb interactions unscreened in the direction perpendicular to the layer make the renormalization of electron interactions huge and the electrostatic energies slowly convergent. Therefore, the supercells have to be sufficiently large to marginalize the periodicity effects and to allow for reliable finite-size extrapolations. To this end, we have carried out extensive calculations of Δ_f for the sequence of 1×1 up to 6×6 periodic supercell systems with two DFT nodal hypersurfaces. For sizes 3×3 or larger the linear scaling describes the results very well. For smaller supercells, the different components of the total energies, such as the potential energy, are too biased to make the trends transparent.

The infinite-size extrapolation from the extended-system calculations yields

$$\Delta_f^{\text{ext},1} = 2.68 \pm 0.10 \text{ eV}, \quad (1)$$

fixing the nodal hypersurfaces by the hybrid B3LYP¹³ DFT functional. Recall that the corresponding DFT

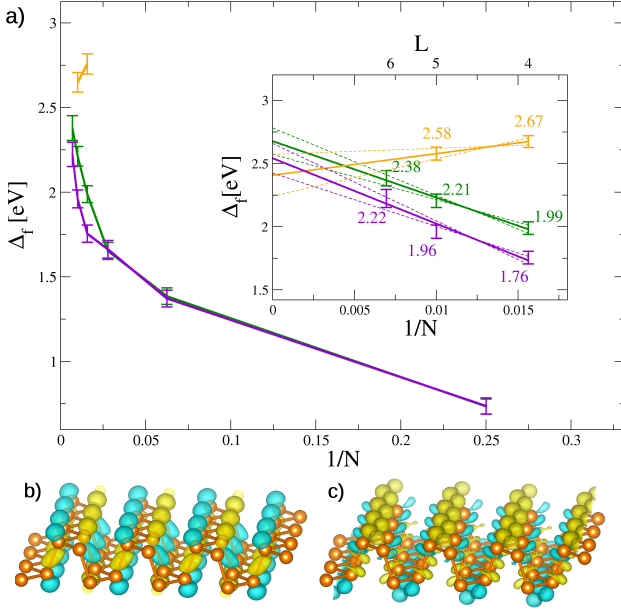


FIG. 2. a) Finite-size scaling of the computed fundamental gap, Δ_f , with the number of atoms, N , in the periodic supercell (green line, DMC/B3LYP; purple line, DMC/PBE) and in the cluster approach (yellow line, DMC/B3LYP) along the series of $L \times L$ supercell approximants, $L = 1$ to 6, for the periodic setup and $L = 4, 5$ in the cluster approach. The inset shows the zoom-in of the scaling for large N with the dashed lines showing the linear extrapolation to the infinite size limit. b) B3LYP DFT HOMO (left) and c) LUMO (right) orbitals. Both are Γ -point Bloch states, HOMO being a superposition of bonding orbitals (mostly $\sigma(p_z)$) along the vertical P-P bonds while LUMO being its antibonding counterpart.

value is 1.7 eV, see Tab. I. If we now fix the nodal hypersurfaces by PBE¹² DFT single-particle orbitals, see Figure 2 a), we get the extrapolation to

$$\Delta_f^{\text{ext},2} = 2.54 \pm 0.12 \text{ eV}, \quad (2)$$

which overlaps with $\Delta_f^{\text{ext},1}$ within the error bars. The PBE DFT gap is 0.8 eV. Remarkably, despite the significant difference of almost 1 eV in the DFT gaps, the QMC method that starts with the corresponding DFT wave functions (and fixing their nodal hypersurfaces), gives a consistent output for both! Surprisingly, the convergence of Δ_f in the periodic setting is determined mainly by the Hartree-Fock energy components, with the rest, including the correlation energies, converging much faster. For example, the ground-state correlation energy is essentially converged at the 3×3 supercell size, whereas the excited-state at a slightly larger size of 5×5 . This provides a way of estimating the phosphorene properties from the more slowly converging Hartree-Fock results, simply by adding the corresponding correlation energies; see SM for more details. We also plot the HOMO/LUMO orbitals for the extended calculations at the Γ point in Fig. 2 b) and c), respectively. The orbital's distribution

and bonding type can give insight into Coulomb finite size effects; see SM for a discussion.

Clusters. Due to intricacies of extrapolations of the periodic supercells, and for consistency, we have also calculated Δ_f in a finite cluster setting. The clusters corresponded to supercell sizes in the periodic method above, with terminations of unsaturated bonds with H atoms, see Fig. 1 c) and d). Finite-size scaling constructed from these cluster approximants, given in Fig. 2 a), extrapolates to

$$\Delta_f^{\text{clst}} = 2.41 \pm 0.17 \text{ eV}, \quad (3)$$

reasonably close to Δ_f^{ext} considering the fact that we compare periodic systems versus isolated clusters in vacuum and that these two models actually exhibit opposite trends as the functions of the system size. Due to finite-size confinement, the computed excitations in finite clusters as a rule overestimate the gaps. The DMC values for the 5×5 clusters clearly illustrate this, see Fig. 2 a). However, as explained in SM, the cluster gaps are bound to converge to the fundamental gap in the infinite size limit and also provide upper bounds for the estimation of fundamental gaps as indicated above. The upper bound property of cluster gaps enables us to probe usefulness of alternative extrapolations to bulk schemes, such as, for instance, $1/\sqrt{N}$ scaling,⁴⁹ see SM. Since both our estimates of Δ_f from the periodic supercells are greater than the cluster estimate, there is likely a small bias in the evaluation of excitations in the periodic supercells. In particular, the fixed-node errors in the excited and the ground states are most likely not identical and could be also intertwined with the remnants of the finite size errors even at larger sizes.

The convergence of the excited states is much more challenging in extended 2D systems than in bulk. The key reason is that the non-periodic direction enables changes in the single-particle densities that have dominant contribution to the periodic Coulomb interactions, a problem that is naturally avoided in cluster geometries; for details see SM. Therefore, we estimate that a systematic uncertainty of 0.1 to 0.2 eV could be present in our periodic-supercells gap calculations. The multiple calculations of the excited states that we present clearly illustrate this aspect.

The error is certainly greater for the excited-state energy, than for the ground state. Since the variational principle behind QMC gives the upper bound on the energy, it follows that the cluster value is a superior estimate for the fundamental gap. We believe that the true value of Δ_f for intrinsic phosphorene is about 2.4 eV, as also indicated in Tab. I. The GW values, defining the current state-of-the-art, are, compared to QMC, widely scattered and systematically underestimating the gap.

Exciton binding energy, optical gap, and comparison with experiment. Using the universal linear scaling,¹⁴ $\Delta_b \approx 0.27\Delta_f$, we can also estimate the excitonic binding energy of phosphorene as $\Delta_b \approx 0.65$ eV. The optical gap is then $\Delta_o = \Delta_f - \Delta_b \approx 1.75$ eV. This is consistent

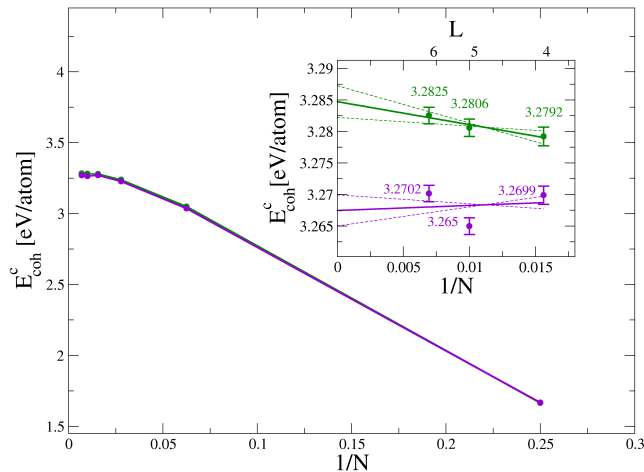


FIG. 3. Finite-size scaling of fixed-node corrected cohesion energy E_{coh}^c , in DMC/PBE (purple curve) and DMC/B3LYP (green curve) treatment. The error bars are smaller than the size of the points. The inset shows the zoom-out of the linear scaling for large N with extrapolation to infinite system size.

with the optical absorption experiment²⁶ which reports 1.73 eV. As we discussed in the introduction, the optical gap of 2D semiconductors should be insensitive to the dielectric environment, justifying the consistency claim.

In terms of the fundamental gap obtained in experiment, (see Tab. I), photoluminescence emission spectroscopy (silicon substrate, no capping),²³ optical absorption (sapphire substrate, h-BN capping),²⁶ and scanning tunneling spectroscopy (no capping),¹⁶ yield values of Δ_f of 2.2, 1.8, and 2.0 eV, respectively. The optical absorption value was attributed to the h-BN capping which also seems to reduce the exciton binding energy to just 0.1 eV.²⁶ The photoluminescence value of 2.2 eV is closest to our QMC prediction. Considering that the sample was on a dielectric substrate which lowers Δ_f by perhaps 0.1–0.2 eV,²⁶ our result is also consistent with this experiment.

Cohesion energy. One important quantity which, to the best of our knowledge, has not been determined experimentally yet, is the free-standing phosphorene cohesion energy. The cohesion energy of bulk black phosphorus is 3.43 eV/atom.⁵⁰ Compared to ordinary semiconducting 3D materials the phosphorus crystal is quite different being a van der Waals system of covalently bonded slabs. Even though the system shows moderately large cohesion, the stability of black phosphorus is rather low mainly due to an easy detachment of P_4 molecular units that per atom are bonded almost as strongly as the bulk material. Having calculated the phosphorene DMC ground state energies for a variety of sizes we can estimate the cohesion energy in the thermodynamic limit. Since the P_4 molecule is the dominant sublimation product from phosphorus solids, to estimate the cohesion we follow the thermodynamic path P_4 molecule \rightarrow bulk black phosphorus \rightarrow phosphorene using also the QMC calcu-

lation of the van der Waals binding energy estimated recently.²⁸ The finite-size scaling, Fig. 3, yields a fixed-node corrected cohesion energy of 3.268(4) in DMC/PBE and 3.284(6) eV/atom in the DMC/B3LYP periodic calculations, while from the clusters the estimated value is 3.26(1) eV/atom, see the SM for more details. Note that our estimated DMC values of cohesion energy of phosphorene from the two models are almost identical and very close to the estimation of 3.35 eV/atom for the 2D system obtained by using the van der Waals interlayer bonding from another DMC calculation.²⁸ The corresponding DFT values are 3.09 eV/atom⁵¹ and 3.45 eV/atom.⁵²

IV. CONCLUSION AND PERSPECTIVES

We have performed systematic fixed-node QMC calculations of the quasiparticle band gap of free-standing single-layer phosphorene in both periodic and cluster settings. Using the universal linear scaling between the gap and the optical binding energy, we have also extracted the optical gap, which can be compared with experiments done on phosphorene on dielectric substrates or on encapsulated samples. Our results are consistent with available optical absorption and photoluminescence emission spectroscopy experiments. We argue that previous calculations based on GW underestimate the quasiparticle gap and do not give consistent predictions for phosphorene. Our ground state is essentially exact, evidenced from the calculated cohesion and its agreement with available (indirect) experimental data.

Our calculated quantities, band gap and cohesion, are key inputs into more qualitative and approximate theories, such as tight-binding and k-p, as well as into experimental interpretations. In particular, there is a clear path how our results can be modified to accommodate dielectric environments which enter the experiments, leaving the core of our QMC results unchanged. This can be done by Bethe-Salpeter modeling or by use of model dielectric screening³⁴ to find the appropriate value of the exciton binding energy. Hence, our explicitly many-body QMC results provide a reference ground for further studies on phosphorene based on strain and layer engineering as well as chemical doping and structural defects and indeed in any other 2D material. We have also demonstrated that these cutting-edge calculations are now feasible for a range of 2D systems and we expect the QMC methods to find a place at the top of the list of the toolkit for studying 2D systems. This is underscored by the fact that the scatter of predicted values for electronic parameters is significant not only in phosphorene, but in other 2D materials as well.^{34,36,53}

ACKNOWLEDGMENTS

R.D., K.T., and I.S. were supported by APVV-15-0759, VEGA-2/0162/15 and VEGA-2/0123/18 projects.

Contributions by L.M. have been supported by the NSF grant DMR-1410639 and by XSEDE computer time allocation at TACC. T.F. was supported by GRK Grant No. 1570, and the International Doctorate Program Topological Insulators of the Elite Network of Bavaria. J. F. acknowledges funding from the European Union's Horizon 2020 research and innovation program under grant agreement No. 696656, and DFG SFB 1277 (B07). Total estimated amount of computation time is in excess of 30 million core hours on current architecture. T. F. and J. F. acknowledge the Gauss Centre for Supercomputing (www.gauss-centre.eu) for funding this project by providing computing time on the GCS

Supercomputer SuperMUC at Leibniz Supercomputing Centre (LRZ, www.lrz.de). R.D., K.T., and I.S. acknowledge that the results of this research have been obtained using the DECI resources Beskow at the PDC Center for High Performance Computing at the KTH Royal Institute of Technology, Stockholm, Sweden from the PRACE project NaM2D and SisU based in Finland at CSC IT Center for Science with support from the PRACE DoCSiNaP project. We also gratefully acknowledge use of the Hitachi SR16000/M1 supercomputer system at CCMS/IMR, Tohoku University, Japan. We also acknowledge useful discussions with Martin Gmitra and Alexey Chernikov.

-
- [1] L. Li, Y. Yu, G. J. Ye, Q. Ge., X. Ou., H. Wu, D. Feng, X. H. Chen., and Y. Zhang, *Nat. Nanotechnol.* **9**, 372 (2014).
 - [2] H. Liu, A. T. Neal, Z. Zhou, Z. Luo, X. Xu, D. Tomanek, and P. D. Ye, *ACS Nano* **8**, 4033 (2014).
 - [3] K. Novoselov, A. Geim, S. Morozov, D. Jiang, Y. Zhang, S. Dubonos, I. Grigorieva, and A. Firsov, *Science* **306**, 666 (2004).
 - [4] B. Hunt, J. D. Sanchez-Yamagishi, A. F. Young, M. Yankowitz, B. J. LeRoy, K. Watanabe, T. Taniguchi, P. Moon, M. Koshino, P. Jarillo-Herrero, and R. Ashoori, *Science* **340**, 1427 (2013).
 - [5] K. F. Mak, C. Lee, J. Hone, J. Shan, and T. F. Heinz, *Phys. Rev. Lett.* **105**, 136805 (2010).
 - [6] K. Watanabe, T. Taniguchi, and K. Hisao, *Nat. Mat.* **3**, 404 (2004).
 - [7] W. Han, R. Kawakami, M. Gmitra, and J. Fabian, *Nat. Nanotechnol.* **9**, 794 (2014).
 - [8] H. Duan, N. Yan, R. Yu, C.-R. Chang, G. Zhou, H.-S. Hu, H. Rong, Z. Niu, and J. Mao, *Nat. Commun.* **5**, 3093 (2014).
 - [9] X. Ling, H. Wang, S. Huang, F. Xia, and M. S. Dresselhaus, *Proc. Natl. Acad. Sci. USA* **112**, 4523 (2015).
 - [10] A. Castellanos-Gomez, *J. Phys. Chem. Lett.* **6**, 4280 (2015).
 - [11] P. Cudazzo, L. Sponza, C. Giorgetti, L. Reining, F. Sottile, and M. Gatti, *Phys. Rev. Lett.* **116**, 066803 (2016).
 - [12] J. P. Perdew, K. Burke, and M. Ernzerhof, *Phys. Rev. Lett.* **77**, 3865 (1996).
 - [13] P. J. Stephens, F. J. Delvin, C. F. Chabalowski, and M. J. Frisch, *J. Phys. Chem.* **98**, 11623 (1994).
 - [14] Z. Jiang, Z. Liu, Y. Li, and W. Duan, *Phys. Rev. Lett.* **118**, 266401 (2017).
 - [15] Y. Cai, G. Zhang, and Y. W. Zhang, *Sci. Rep.* **4**, 6677 (2014).
 - [16] L. Liang, J. Wang, W. Lin, B. G. Sumpter, V. Meunier, and M. Pan, *Nano Lett.* **14**, 6400 (2014).
 - [17] V. Wang, Y. Kawazoe, and W. T. Geng, *Phys. Rev. B* **91**, 045433 (2015).
 - [18] J. H. Choi, P. Cui, H. Lan, and Z. Zhang, *Phys. Rev. Lett.* **115**, 066403 (2015).
 - [19] F. A. Rasmussen, P. S. Schmidt, K. T. Winther, and K. S. Thygesen, *Phys. Rev. B* **94**, 155406 (2016).
 - [20] V. Tran, R. Soklaski, Y. Liang, and L. Yang, *Phys. Rev. B* **89**, 235319 (2014).
 - [21] A. N. Rudenko and M. I. Katsnelson, *Phys. Rev. B* **89**, 201408(R) (2014).
 - [22] F. Ferreira and R. M. Ribeiro, *Phys. Rev. B* **96**, 115431 (2017).
 - [23] X. Wang, A. Jones, K. Seyler, V. Tran, Y. Jia, H. Zhao, H. Wang, L. Yang, X. Xu, and F. Xia, *Nat. Nanotechnol.* **10**, 517 (2015).
 - [24] A. Surrente, A. A. Mitoglu, K. Galkowski, W. Tabis, D. K. Maude, and P. Plochocka, *Phys. Rev. B* **93**, 121405(R) (2016).
 - [25] G. Zhang, S. Huang, A. Chaves, C. Song, O. Özçelik, T. Low, and H. Yan, *Nat. Commun.* **8**, 14071 (2016).
 - [26] L. Li, J. Kim, C. Jin, G. J. Ye, D. Y. Qiu, F. H. da Jornada, Z. Shi, L. Chen, Z. Zhang, F. Yang, K. Watanabe, T. Taniguchi, W. Ren, S. G. Louie, X. H. Chen, Y. Zhang, and F. Wang, *Nat. Nanotechnol.* **12**, 21 (2017).
 - [27] F. Xia, H. Wang., and Y. Jia, *Nat. Commun.* **5**, 4458 (2014).
 - [28] L. Shulenburg, A. D. Baczewski, Z. Zhu, J. Guan, and D. Tománek, *Nano Lett.* **15**, 8170 (2015).
 - [29] R. Roldán, A. Castellanos-Gomez, E. Capelluti, and F. Guinea, F. Guinea, *J. Phys.: Condens. Matter* **27**, 313201 (2015).
 - [30] K. Tokár, R. Derian, J. Brndiar, and I. Štich, *J. Appl. Phys.* **120**, 194305 (2016).
 - [31] J. Xiao, M. Zhao, Y. Wang, and X. Zhang, *Nanophotonics* **6**, 1309 (2017).
 - [32] S. Latini, T. Olsen, and K. S. Thygesen, *Phys. Rev. B* **92**, 245123 (2015).
 - [33] A. V. Stier, N. P. Wilson, G. Clark, X. Xu, and S. A. Crooker, *Nano Lett.* **16**, 7054 (2016).
 - [34] M. L. Trolle, T. G. Thomas G. Pedersen, and V. Vénard, *Sci Rep.* **7**, 39844 (2017).
 - [35] A. Raja, A. Chaves, J. Yu, G. Arefe, H. M. Hill, A. F. Rigosi, T. C. Berkelbach, P. Nagler, C. Schiller, T. Korn, C. Nuckolls, J. Hone, L. E. Brus, T. F. Heinz, D. R. Reichman, and A. Chernikov, *Nature Commun.* **8**, 15251 (2017).
 - [36] Y. Cho and T. C. Berkelbach, *Phys. Rev. B* **97**, 041409(R) (2018).
 - [37] C. Wang, Q. Xia, Y. Nie, and G. Guob, *J. Appl. Phys.* **117**, 124302 (2015).
 - [38] W. M. C. Foulkes, L. Mitás, R. J. Needs, and G. Rajagopal, *Rev. Mod. Phys.* **73**, 33 (2001).

- [39] R. J. Needs, M. D. Towler, N. D. Drummond, and P. López Ríos, *J. Phys.: Condens. Matter* **22**, 023201 (2010).
- [40] J. Kolorenč and L. Mitás, *Rep. Prog. Phys.* **74**, 026502 (2011).
- [41] L. K. Wagner and D. M. Ceperley, *Rep. Prog. Phys.* **79**, 094501 (2016).
- [42] M. Dubecký, L. Mitás, and P. Jurecka, *Chem. Rev.* **116**, 5188 (2016).
- [43] L. Horváthová, M. Dubecký, L. Mitás, and I. Štich, *Phys. Rev. Lett.* **109**, 053001 (2012).
- [44] R. Derian, K. Tokár, B. Somogyi, Á. Gali, and I. Štich, *J. Chem. Theory Comput.* **13**, 6061 (2017).
- [45] E. Mostaani, N. D. Drummond, and V. I. Fal'ko, *Phys. Rev. Lett.* **115**, 115501 (2015).
- [46] P. Li and I. Appelbaum, *Phys. Rev. B* **90**, 115439 (2014).
- [47] I.-C. Yeh and M. L. Berkowitz, *J. Chem. Phys.* **111**, 3155 (1999).
- [48] B. Wood, W. M. C. Foulkes, M. D. Towler, and N. D. Drummond, *J. Phys.: Condens. Matter* **16**, 891 (2004).
- [49] N. D. Drummond, V. Zólyomi, and V. I. Fal'ko, *Electronic Structure of Two-Dimensional Crystals of Hexagonal Boron Nitride* (TTI, QMC in the Apuan Alps VIII, Vallico Sotto, Tuscany, Italy, 2013) http://www.tcm.phy.cam.ac.uk/~mdt26/tti_talks/qmcitaa_13/drummond.tti2013.pdf.
- [50] C. Kittel, *Introduction to Solid State Physics*, 8th ed. (John Wiley & Sons, Inc., NJ, 2005) p. 50.
- [51] P. Ballone and R. O. Jones, *J. Chem. Phys.* **100**, 4941 (1994).
- [52] P.-J. Chen and H.-T. Jeng, *Sci. Rep.* **6**, 23151 (2016).
- [53] J. Ryou, Y.-S. Kim, K. C. Santosh, and K. Cho, *Sci. Rep.* **6**, 29184 (2016).

Supplementary Information to: Many-body quantum Monte Carlo study of 2D materials: cohesion and band gap in single-layer phosphorene

T. Frank,¹ R. Derian,² K. Tokár,² L. Mitas,³ J. Fabian,^{1,*} and I. Štich^{2,4,5,†}

¹*University Regensburg, Institute for Theoretical Physics, 93040 Regensburg, Germany*

²*Center for Computational Materials Science, Institute of Physics,
Slovak Academy of Sciences, 84511 Bratislava, Slovakia*

³*Department of Physics, North Carolina State University, Raleigh, NC 27695-8202*

⁴*Institute of Informatics, Slovak Acad. of Sciences, 845 07 Bratislava, Slovakia*

⁵*Department of Natural Sciences, University of Ss. Cyril and Methodius, 917 01 Trnava, Slovakia.*

I. SIMULATION DETAILS

The electronic fundamental band gaps Δ_f , were determined for both, extended and cluster systems with B3LYP¹ DFT orbitals and also extended systems with PBE^{2,3} DFT orbitals. Lattice parameters were fixed to the experimental values of black phosphorus crystal^{4,5}.

The fixed-node QMC^{6,7} electronic gap calculations were performed in three steps:

- 1) the trial wave functions for ground- and excited-states were constructed from DFT B3LYP¹ and PBE^{2,3} single-particle DFT wave functions. Note that, unlike the GGA-type PBE, the hybrid B3LYP functional yields a fairly realistic band gap of 1.7 eV already at the DFT level (see Table I of the main text). Note also that no charge transfer is associated with the HOMO→LUMO transition, indicating that range-separated hybrids, such as CAM-B3LYP functional⁸, may not be needed.
- 2) the ground state trial wave function constructed from the DFT wave functions was optimized using VMC (variational Monte Carlo) techniques, and
- 3) finally fundamental gaps were computed from DMC (diffusion Monte Carlo) energies of ground- and excited-states as first singlet-singlet vertical excitation energies, where always the Jastrow factor of the ground state was used:

$$\Delta_f \approx E_v^s = E_1^s - E_0^s \quad ,$$

with E_0 , E_1 being, respectively, the ground- and the first excited-states obtained by fixed-node DMC⁶ (PBE/DMC and B3LYP/DMC) not allowing any relaxation of the DFT nodal hypersurfaces due to the HOMO→LUMO electron excitation.

Our QMC gap estimates use the vertical transition approximation, i.e. they neglect all the adiabatic, vibronic and zero-point vibrational energy effects. Such approximations tend to increase the gap value compared to the experiments, but on much smaller scale than that of importance here.

For DFT modeling we use the CRYSTAL code⁹, while for all VMC and DMC calculations the QWalk code¹⁰ was used. In all calculations the atomic cores were replaced by effective core potentials (ECP)¹¹ used in combination with a VTZ basis set.

Dynamical correlations were explicitly built in into the trial wave functions via isotropic Schmidt-Moskowitz Jastrow factors^{7,12}, including electron-electron and electron-nucleus correlations. Parameters of the trial wave functions⁷ were optimized by minimizing linear combination of energy and variance¹³. The T-moves scheme¹⁴ was used to keep the calculations with ECPs variational. Our systems are 2D+h in nature, i.e. while being 2D, they also have a finite thickness h. In order to take that structural characteristics into account, the Yeh-Berkowitz¹⁵ modification of 3D Ewald summation technique for systems with a slab geometry that are periodic in two dimensions and have a finite length in the third dimension was adopted.

Two different types of finite-size scaling were performed:

- 1) a series of $L \times L$ supercell approximants where L goes from 1 to 6, see Figure 1 of the main text, and
- 2) 4×4 and 5×5 H-terminated cluster approximants, see Figure 1 of the main text.

More details of the finite-size scaling are given in Sec. III.

The choice of these two types of models (periodic and finite) was driven by difficulties in estimating the band gap in the periodic setting. As explained and demonstrated below on solid data, the periodic calculations for excited states converge to the thermodynamic limit very slowly. Remarkably, we find that the cluster models converge to the infinite limit much faster and with much smaller variations of extrapolated estimators.

II. COHESION ENERGY

We start the estimate of the cohesion energy from the P₄ molecule that by bonding patterns and energetics is very close to white and red phosphorus bulk crystals. P₄ is also the dominant sublimation product from phosphorus solids. Therefore we will use the following thermodynamic path molecule P₄ ↔ black phosphorus bulk ↔ phosphorene to find the cohesion. For P₄ binding we

* jaroslav.fabian@ur.de

† ivan.stich@savba.sk

initially use very accurate calculations and experimental data from the W4 testing set¹⁶. Coupled Cluster extrapolation to infinite basis and also experiment give an atomization energy of 285.03 kcal/mol (experiment being within 1 kcal/mol) and a zero point energy (ZPE) of 0.98 kcal/mol per atom. Our best Coupled Cluster extrapolated estimation is within 1.5 kcal/mol of the W4 value, see Table I. We also estimate the core-valence correlation and relativity corrections of -0.4 kcal/mol per atom¹⁷ from calculations of P_2 . Therefore the P_4 atomization energy (bottom of the well, infinitely heavy nuclei) at $T = 0$ K is 286.95 kcal/mol or 3.110(9) eV/atom.

Cohesion of the bulk black phosphorus can be estimated from the sublimation energy of black phosphorus ($P_4 \rightarrow \text{gas}(P_4)$). We take a value of the heat of sublimation of 25.5(2.5) kJ/mol per atom or 0.26 eV/atom¹⁸ (or almost the same value from an alternative experiment that estimates the cohesion energy difference between white and black bulks to be 21.2(2.5) kJ/mol and the heat of sublimation from white phosphorus to gas of 3.4 kcal/mol per P_4 ¹⁹ so that we sum it to 25.5(2.5) kJ/mol = 0.26 eV/atom). Therefore the bulk black phosphorus cohesive energy with infinitely heavy nuclei is about 3.37(9) eV/atom (we assume that ZPE/atom is the same as in P_4 and this assumption also increases the error bar).

Bulk black phosphorus consists of stacked layers of phosphorene that are bounded by ≈ 0.08 eV/atom⁵. Therefore a reasonable estimate for phosphorene cohesion that we can infer from this data is

$$E_{\text{coh}, T \approx 0, \infty \text{ nuclei}}^{\text{phosphorene}} = 3.29(9) \text{ eV/atom.}$$

We neglected relaxation of phosphorene layer in vacuum as compared to the layers in black phosphorus bulk but that is probably within the approximately estimated error bar.

Let us now analyze the fixed node diffusion Monte Carlo (FNDMC) calculations and results. Single FNDMC atom with PBE DFT orbitals, Burkatzki-Filippi-Dolg pseudopotentials²⁰, and single reference is

$$E_{\text{PBE FNDMC}}^{\text{single atom}} = -6.4740(4) \text{ Ha}$$

or

$$E_{\text{B3LYP FNDMC}}^{\text{single atom}} = -6.4737(4) \text{ Ha}$$

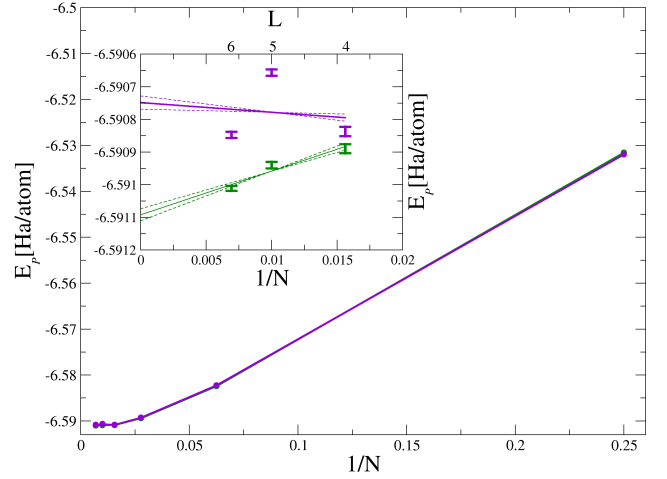
with B3LYP nodal hypersurfaces.

Results of the FNDMC phosphorene supercell calculations are shown in Supplementary Figure. 1 and the $N \rightarrow \infty$ extrapolated per atom energy is

$$\begin{aligned} E_{\text{PBE FNDMC}}^{\text{phosphorene}} &= -6.59074(2) \text{ Ha} \rightarrow \\ E_{\text{coh PBE FNDMC}} &\approx 3.178(2) \text{ eV/atom} \end{aligned}$$

with PBE nodal hypersurfaces and

$$\begin{aligned} E_{\text{B3LYP FNDMC}}^{\text{phosphorene}} &= -6.59109(2) \text{ Ha} \rightarrow \\ E_{\text{coh B3LYP FNDMC}} &\approx 3.194(3) \text{ eV/atom} \end{aligned}$$



Supplementary Figure 1. Finite-size scaling of fixed-node DMC energy per atom in phosphorene in PBE/DMC (purple line) and B3LYP/DMC (green line) treatments. The error bars are smaller than the size of the points. The inset shows the zoom-in of the linear scaling for large N with extrapolation to infinite system size.

Supplementary Table I. Basis set dependence and complete basis set (CBS) limit of CCSD(T) energies determined with Burkatzki-Filippi-Dolg pseudopotentials²⁰, in Hartree energies, of the P atom and the P_4 cluster.

basis set	P atom	P_4 cluster
cc-pVTZ	-6.468765433	-26.28345057
cc-pVQZ	-6.475058531	-26.34037340
cc-pV5Z	-6.476654877	-26.35692173
CBS	-6.477197450	-26.36370441

with B3LYP nodal hypersurfaces.

Both energies have fixed-node errors. We approximately estimate them from results of exact CCSD(T) in complete basis set limit (CBS) for the P atom and P_4 cluster since its cohesion/binding and bonding patterns are similar to phosphorene. The results of Burkatzki-Filippi-Dolg pseudopotential²⁰ calculations for a P atom and a P_4 cluster are in Supplementary Table I. To estimate the fixed-node error we need, in addition to the DMC atomic energies, also the P_4 energies, which we calculate as:

$$E_{\text{PBE FNDMC}}^{P_4} = -26.3376(2) \text{ Ha}$$

and

$$E_{\text{B3LYP FNDMC}}^{P_4} = -26.3365(2) \text{ Ha}$$

for PBE and B3LYP nodal hypersurfaces, respectively.

This gives the fixed-node errors of 0.095 eV/atom (0.088 eV/atom) and 0.185 eV/atom (0.178 eV/atom) in the atom and P_4 cluster with B3LYP (PBE) nodal hypersurfaces, respectively. Therefore we assume the FN differential error correction by about $(0.178 - 0.088)$ eV/atom = 0.09 eV/atom at the PBE/DMC level and $(0.185 - 0.095)$ eV/atom = 0.09 eV/atom at the B3LYP/DMC. Our corrected estimate of the cohesion energy is:

$$E_{\text{coh,PBE FNDMC,FN-corrected}} = 3.268(4) \text{ eV/atom},$$

and

$$E_{\text{coh,B3LYP FNDMC,FN-corrected}} = 3.284(6) \text{ eV/atom},$$

where the uncertainty is coming fully from the fixed-node correction since the statistical error bars are well below this. These fixed-node corrected cohesion energies compare also favorably with the estimate of 3.29(9) eV/atom given in the introduction.

III. FINITE-SIZE SCALING

A. HOMO-LUMO and Δ_f gap

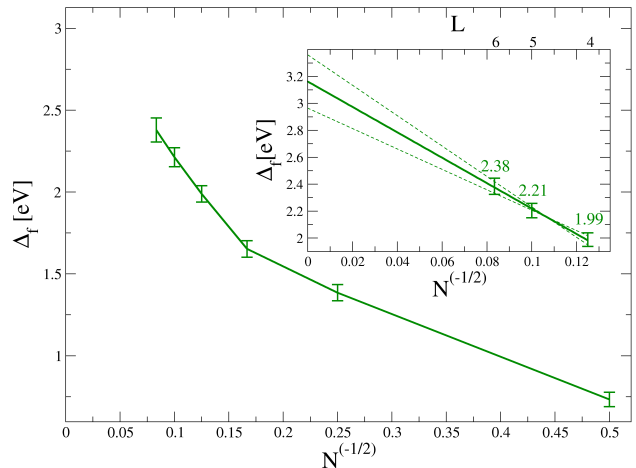
The fundamental gap can be determined from total energies as⁶:

$$\Delta_f = (E_{N_e+1} - E_{N_e}) - (E_{N_e} - E_{N_e-1}) \quad (1)$$

with N_e being the number of electrons. In the GGA approximation, Δ_f converges to the DFT HOMO-LUMO gap in the $N_e \rightarrow \infty$ limit and demonstrates that in the infinite limit at the DFT GGA level there is no interaction between the electron and the hole in the exciton and the HOMO-LUMO gap corresponds to the fundamental gap, Δ_f . Such a conclusion is also valid in the generalized Kohn-Sham theory²¹, i.e. also for hybrid functionals used in the main text. This is a key property for understanding our QMC cluster results in the main text. However, since the LUMO level is constructed identically for finite and infinite systems, the DMC cluster results will, in the infinite system size limit, converge to the true DMC value of Δ_f . In addition, due to the confinement of the excitation, which can only increase the band gap, the cluster results will provide a strict upper limit for our extended system results.

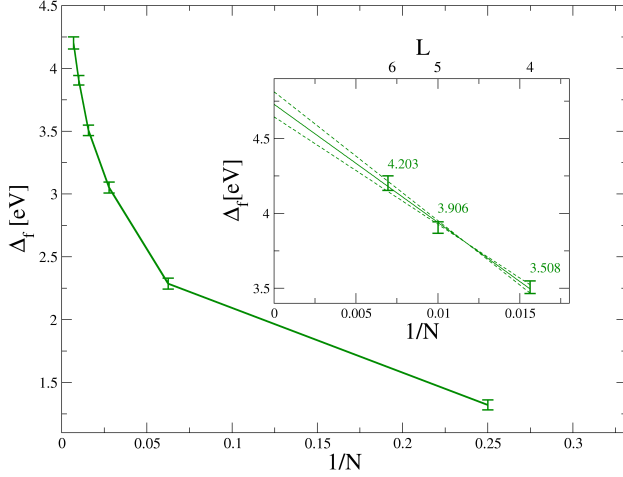
B. Finite size scaling of QMC gaps

An analytical formula for the asymptotic finite-size scaling of the band gap is not known. In the main text we use the scaling versus $1/N$. However, our calculated gap values could equally well be fitted with other fitting formulas, such as for instance with any $1/\sqrt[N]{N}$ formula. For example Drummond²² used $1/\sqrt[3]{N}$. Indeed, fitting



Supplementary Figure 2. Finite-size scaling of DMC/B3LYP fundamental gap, i.e. the gap values from Figure 2 of the main text, versus $1/\sqrt{N}$. Inset shows a zoom and extrapolation for the three largest supercells.

our data versus $1/\sqrt[3]{N}$, Supplementary Figure 2, yields a fit that extrapolates to Δ_f of 3.08 eV. This, though, is in disagreement with the upper bound provided by the cluster calculations which exclude any higher root extrapolation than 1, i.e., the linear finite-size extrapolation versus $1/N$ is used in the main text. Further analysis of the behavior for larger sizes supports these conclusions and provides therefore a rather solid estimation. This is further supported by the analysis of the cohesion energy that shows that the ground state is converged at sizes 4×4 or larger (see main text Fig. 3). The convergence of the excited state in periodic setting is slower due to the presence of vacuum in the direction orthogonal to the phosphorene slab. This enables uninhibited restructuring of the charge in this direction and thus generates long-range (artificial) interactions. In particular, the excited state, as it is clear from Figure 2 of the main text, shows basically an antibonding pattern along one of the P-P bonds that is almost orthogonal to the phosphorene plane (xy -direction) and therefore possesses a significant tail in the z -direction. The excited state is then a repetition of the same bonding pattern at all symmetry-related bonds since the excitation corresponds to the Γ -point symmetry. This results in arrays of dipoles on both sides of the slab and contributes significantly to the potential energy. Indeed, this is amply visible in the corresponding HF energies for the excited states (see Sec. C). The convergence to the thermodynamic limit is therefore very slow and extrapolation is quite difficult and very demanding on computational resources.



Supplementary Figure 3. Finite-size scaling of the Hartree-Fock fundamental gap versus $1/N$. Inset shows a zoom and extrapolation for the three largest supercells.

C. Hartree-Fock band gaps

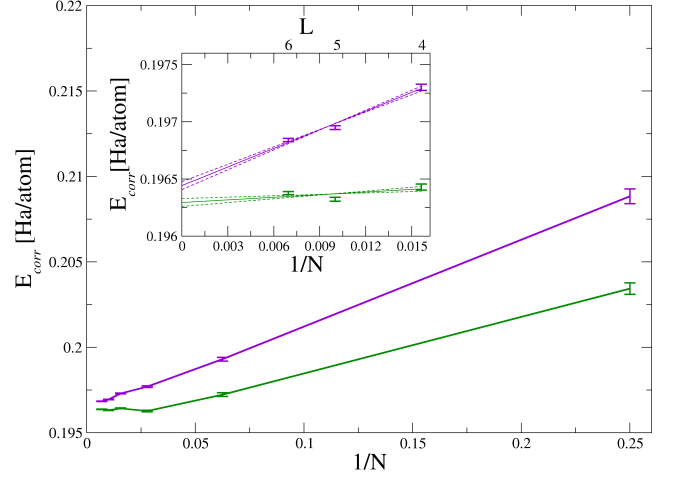
The main contribution to the band gap, the Hartree-Fock part, is plotted in Supplementary Figure 3. This was calculated from the VMC wave function with B3LYP orbitals, setting the Jastrow correlation factor to 1. The Hartree-Fock band gap is extrapolated to 4.720(80) eV in the infinite size limit.

D. Finite-size scaling of correlation energies

Finite-size scaling of correlation energies of both ground- and excited-states are shown in Supplementary Figure 4. The correlation energy of the ground-state are essentially converged at the 4×4 supercell size while that of the excited state appears to converge more slowly but also appears to show sign of being converged for the 6×6 supercell size. The finite-size extrapolated values of correlation energies are 0.19629(3) Ha/atom and 0.19644(3) Ha/atom for the ground- and excited state, respectively. Since the correlation energies converge faster than the Hartree-Fock energies, see Supplementary figure 3, larger approximants could be constructed simply by adding the correlation energies to the Hartree-Fock energies.

IV. EXTRAPOLATIONS BASED ON CALCULATED CORRELATION ENERGIES

Having shown in Sec. III D that the correlation energies tend to saturate at smaller system sizes than the Hartree-Fock energies, we now show that this fact may be used to estimate energies and band gaps for larger approximants. We applied this idea to the 6×6 approximant in



Supplementary Figure 4. Finite-size scaling of the correlation energies of the ground-state S_0 (green line) and the first excited-state S_1 (purple line) versus $1/N$.

the cluster B3LYP/DMC treatment. From the smaller 4×4 and 5×5 DMC cluster calculations the (converged) correlation energies per P and H atom can be estimated, provided the Hartree-Fock energies are also known, Supplementary Table II. The relevant numbers are compiled in Supplementary Table II. From the energies compiled in the Supplementary Table II we estimate a fundamental gap of $\Delta_f^{6 \times 6, \text{clst}, \text{est}} = 2.580(150)$ eV, which is almost within the error bar of the extrapolated value. It confirms that the band gaps of the clusters beyond 4×4 are much more weakly dependent on the size. This enables us to cross check the values from periodic calculations that show much stronger variation with the system size.

Consistency of cluster and periodic calculations can be ascertained also for the total energies per atom and the subsequent cohesion estimation. For clusters $L \times L$ we can use the following total energy model $E_L = N_P E_P + N_H E_H$ that adds energies of corresponding numbers of P and H atoms (see Table II). Based on this we can find linear relationships between different E_L such as, for example, $E_6 = (12/5)E_5 - (3/2)E_4$, etc. Influence of finite sizes is as we mentioned much smaller for clusters than for the periodic calculations. The data enables us therefore to estimate the corresponding total energy per P atom in the thermodynamic limit also in the cluster setting giving the following value

$$E_{\text{FNDMC B3LYP}}^{\text{phosphorene, cluster}} = \frac{1}{80}(4E_5 - 5E_4) = -6.5904(1) \text{ Ha}$$

It compares very favorably with the result from our periodic calculations (compare Sec. II, difference ≈ 0.02 eV/atom) and shows thus remarkably close agreement between these estimations despite significant difference in boundary conditions of the two models.

Supplementary Table II. Total and correlation energies of the ground- (GS) and excited-state (ES) for clusters, in Ha. The Hartree-Fock energies were calculated from Slater determinants with B3LYP orbitals via VMC, setting the Jastrow factor to 1. Bold numbers are estimated values based on computed energies of smaller, 4×4 and 5×5 clusters.

L	# atoms		total energy		HF energy		correlation energy	
	P	H	GS	ES	GS	ES	GS	ES
4	64	24	-435.9029(9)	-435.8046(8)	-423.2858(7)	-423.1230(7)	12.6171(16)	12.6816(15)
5	100	30	-676.6902(10)	-676.5955(9)	-657.0435(10)	-656.8789(10)	19.6467(20)	19.7166(19)
6	144	36	-970.1994(40)	-970.1043(39)	-941.9730(13)	-941.8069(13)	28.2264(37)	28.2974(36)

Supplementary Table III. Tabulated values of calculated band gaps in eV. The Hartree-Fock values correspond to band gaps calculated from B3LYP wave functions via VMC setting the Jastrow factor to 1.

L	1	2	3	4	5	6	∞
HF@B3LYP-periodic	1.320(40)	2.390(44)	3.140(44)	3.510(42)	3.890(38)	4.250(48)	4.720(80)
HF@B3LYP-cluster	-	-	-	4.430(27)	4.480(38)	4.520(52)	4.580(80)
DMC@B3LYP-periodic	0.730(44)	1.390(49)	1.650(50)	1.990(50)	2.210(53)	2.380(60)	2.680(100)
DMC@PBE-periodic	0.740(48)	1.370(49)	1.660(52)	1.760(50)	1.960(53)	2.220(71)	2.540(120)
DMC@B3LYP-cluster	-	-	-	2.670(47)	2.580(52)	-	2.410(170)

V. TABULATED DMC GAPS

All computed gap values are compiled in Supplementary Table III.

-
- [1] P. J. Stephens, F. J. Delvin, C. F. Chabalowski, and M. J. Frisch, "Ab Initio Calculation of Vibrational Absorption and Circular Dichroism Spectra Using Density Functional Force Fields," *J. Phys. Chem.* **98**, 11623–11627 (1994).
- [2] J. P. Perdew, K. Burke, and M. Ernzerhof, "Generalized Gradient Approximation Made Simple," *Phys. Rev. Lett.* **77**, 3865 (1996).
- [3] J. P. Perdew, K. Burke, and M. Ernzerhof, "ER-RATA: Generalized Gradient Approximation Made Simple," *Phys. Rev. Lett.* **78**, 1396 (1997).
- [4] A. Brown and S. Rundqvist, "Refinement of the crystal structure of black phosphorus," *Acta Cryst.* **19**, 684–685 (1965).
- [5] L. Shulenburger, A. D. Baczewski, Z. Zhu, J. Guan, and D. Tománek, "The Nature of the Interlayer Interaction in Bulk and Few-Layer Phosphorus," *Nano Lett.* **15**, 8170–8175 (2015).
- [6] W. M. C. Foulkes, L. Mitás, R. J. Needs, and G. Rajagopal, "Quantum Monte Carlo simulations of solids," *Rev. Mod. Phys.* **73**, 33–83 (2001).
- [7] M. Bajdich and L. Mitás, "Electronic Structure Quantum Monte Carlo," *Acta Phys. Slov.* **59**, 81–168 (2009).
- [8] T. Yanai, D. P. Tew, and N. C. Handy, "A new hybrid exchange-correlation functional using the Coulomb-attenuating method (CAM-B3LYP)," *Chem. Phys. Lett.* **393**, 51–57 (2004).
- [9] R. Dovesi, V. R. Saunders, C. Roetti, R. Orlando, C. M. Zicovich-Wilson, F. Pascale, B. Civalleri, K. Doll, N. M. Harrison, I. J. Bush, Ph. D'Arco, M. Llunell, M. Causà, and Y. Noël, *CRYSTAL14 User's Manual* (University of Torino, Torino, 2014).
- [10] L. Wagner, M. Bajdich, and L. Mitás, "QWalk: A quantum Monte Carlo program for electronic structure," *J. Comp. Phys.* **228**, 3390–3404 (2009), <http://www.qwalk.org>.
- [11] M. Burkatzki, C. Filippi, and J. Dolg, "Energy-consistent pseudopotentials for quantum Monte Carlo calculations," *J. Chem. Phys.* **126**, 234105 (2007).
- [12] K. E. Schmidt and J. W. Moskowitz, "Correlated Monte Carlo wave functions for the atoms He through Ne," *J. Chem. Phys.* **93**, 4172 (1990).
- [13] C. Filippi and C. J. Umrigar, "Energy and Variance Optimization of Many-Body Wave Functions," *Phys. Rev. Lett.* **94**, 150201 (2005).
- [14] M. Casula, "Beyond the locality approximation in the standard diffusion Monte Carlo method," *Phys. Phys. B* **74**, 161102(R) (2006).
- [15] I.-Ch. Yeh and M. L. Berkowitz, "Ewald summation for systems with slab geometry," *J. Chem. Phys.* **111**, 3155–3162 (1999).
- [16] A. Karton, S. Daon, and J. M. L. Martin, "W4 thermochemistry of P-2 and P-4. Is the CODATA heat of formation of the phosphorus atom correct?" *Mol. Phys.* **105**, 2499–2505 (2007).

- [17] D. Feller and K. A. Peterson, “Re-examination of atomization energies for the Gaussian-2 set of molecules,” *J. Chem. Phys.* **110**, 8384–8396 (1999).
- [18] P. A. G. O’Hare, B. M. Lewis, and I. Shirotni, “Thermodynamic stability of orthorhombic black phosphorus,” *Thermochimica Acta* **129**, 57–62 (1988).
- [19] P. A. G. O’Hare and W. N. Hubbard, “Fluorine Bomb Calorimetry,” *Trans. Faraday Soc.* **62**, 2709–2715 (1966).
- [20] M. Burkatzki, C. Filippi, and M. Dolg, “Energy-consistent pseudopotentials for quantum Monte Carlo calculations,” *J. Chem. Phys.* **126**, 234105 (2007).
- [21] J. P. Perdew, W. Yang, K. Burke, Z. Yang, E. K. U. Gross, M. Scheffler, G. E. Scuseria, T. M. Henderson, I. Y. Zhang, A. Ruzsinszky, H. Peng, J. Sun, E. Trushin, and A. Görling, “Understanding band gaps of solids in generalized Kohn Sham theory,” *Proc. Natl. Acad. Sci. USA* **114**, 2801–2806 (2017).
- [22] N. D. Drummond, V. Zólyomi, and V. I. Fal’ko, *Electronic Structure of Two-Dimensional Crystals of Hexagonal Boron Nitride* (TTI, QMC in the Apuan Alps VIII, Vallico Sotto, Tuscany, Italy, 2013) http://www.tcm.phy.cam.ac.uk/~mdt26/tti_talks/qmcitaa_13/drummond.tti2013.pdf.